Nonlinear Dynamics and Chaos

Curtis Hu[1] and Sanaz Mizbani[1]

[1]Department of Physics, UC Berkeley

Abstract.

Period doubling behavior is found in many aspect of scientific experiments. The one-dimensional maps in the simple Logistic Map case as a bridge to study these chaotic systems found in all walks of life. These universal chaotic behaviors can be studied in diode PN junctions of nonlinear circuits as well as a digital circuit analog for a Newtonian bouncing ball. We shall use these systems to understand period cycles, Poincare maps, chaotic regimes, and information entropy.

Key words: Nonlinear Dynamics; Bifurcation; Bouncing Ball Experiment; Cob Web Analysis

1. Introduction

In this experiment, we will be exploring the core concepts of chaos theory which is exploring systems that appear random but are governed by deterministic laws. We explore the concepts of the physical systems being studied such as PN-junctions which act as one way valves for electricity and electric currents. Another example of a physical system being studied is a bouncing ball experiment where using electronic concepts we replicate the motion of a bouncing ball by manipulating the timing between pulses to replicate bounces. Our ultimate goal for this lab is to find theoretical and experimental understanding of the nonlinear systems where outputs are not proportional to the inputs.

1.1. Theory

1.1.1 Logistic Map

A traditional model of population growth uses the following:

$$x_{n+1} = rx_n(1 - x_n) \tag{1}$$

Where r is the reproduction rate. Normally, this is set low enough ($1 \leq r < 3$) such that we achieve our normal S-curve logistic population model – stabilizes into a fixed population. Or it is so low ($0 \leq r < 1$) that the population goes extinct.

However, if we continue to increase the value of r we'll see interesting behavior.

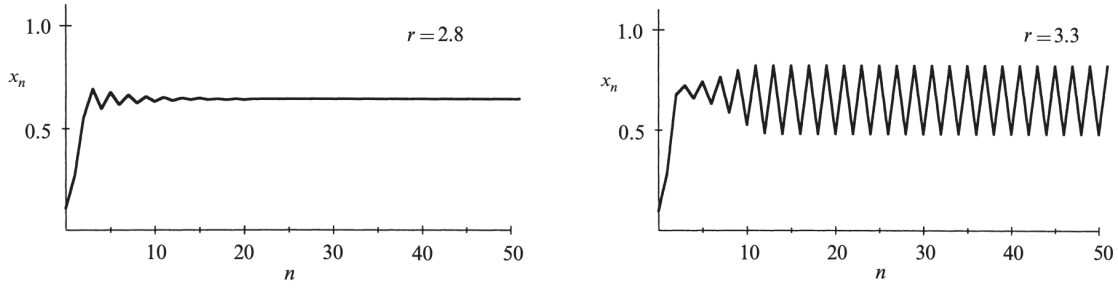

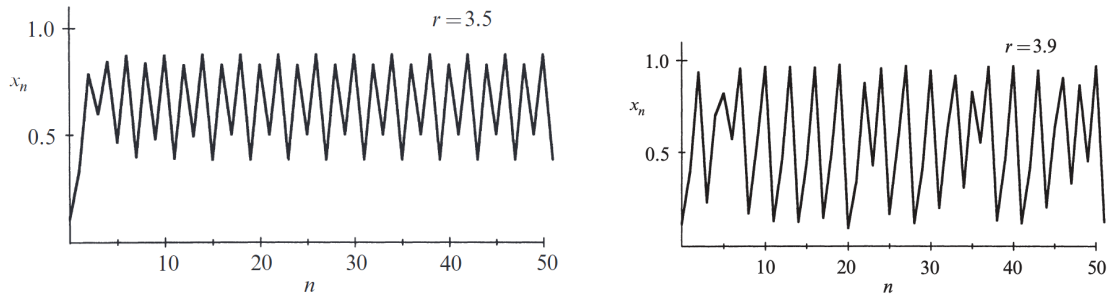

Figure 1: Increasing the chaotic parameter r reveals particular oscillations. Taken from [5]

As you can see, as you increase the value of r, we get period-2 cycles then period-4 cycles and eventually complete chaos.

We find ourselves with 2^n cycle. These bifurcations continue to occur: 2, 4, 8, 32 period cycles.

r	Period Cycle
3	2
3.449...	4
3.54409...	8
3.5644...	16
3.568759...	32
3.569946...	∞

Table 1: Logistic Map Period Cycles

We can graph the x v. r to get the all famous logistic map. For example, we can see the initial two cycles before $r = 3.449....$

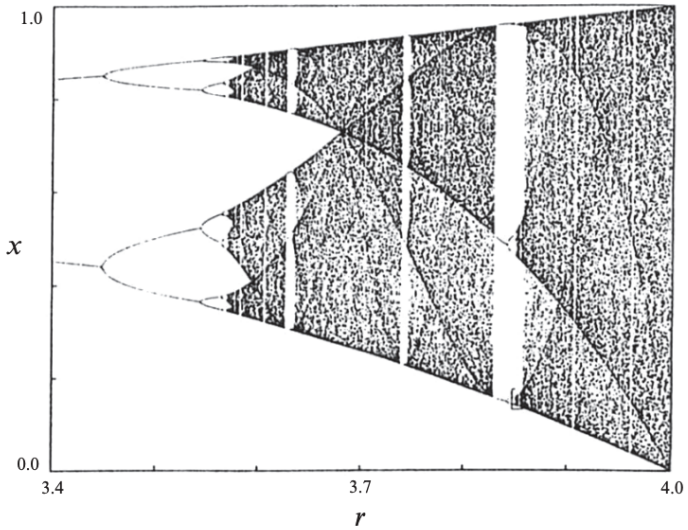

Figure 2: Logistic map from adjusting the chaotic parameter within this specific range

In fact, Feigenbaum shows that there exists a class of functions such that exibiti 'Universal Chaotic Behavior' [1]. Most interestingly, these period doubling systems can be categorized under an umbrella with unifying characteristics. Period doubling is then a characteristic route for a system to follow as it changes over from simple periodic to complex aperiodic motion.

In the limit of aperiodic behavior, there is a unique and hence universal solution common to all systems undergoing period doubling. We call this the Feigenbaum ratio which is formally presented as:

$$\delta_n = \frac{\Lambda_{n+1} - \Lambda_n}{\Lambda_{n+2} - \Lambda_{n+1}} [6]$$

They found that all these systems demonstrate the same constant ratio:

$$\delta = 4.6692016...$$

1.1.2 Cob Web Analyzers

We formally introduce the one-dimensional map which simply iteratively maps a value to it's next:

$$x_{n+1} = f(x_n) \tag{2}$$

We've already seen an example of this in the previous section on logistic maps in eq. 1. (Sometimes this can be a discretized sample of $\dot{x} = f(x)$ to which we call this the **Poincare Map** $x_{n+1} = P(x_n)$ over the **Poincare section**.) Depending on the function $f(x_n)$, certain points x^* can be stable or unstable. More intuitively, nearby points can either be flowing towards x^* or away from x^* under eq. 2. More formally, a nearby point $x^* + \eta$ can under go:

$$\cancel{x^*} + \eta_{n+1} = x_{n+1} = f(x^* + \eta_n) = \cancel{f(x^*)} + f'(x^*)\,\eta_n + O(\eta_n^2)$$
$$\eta_{n+1} = f'(x^*)\eta_n + \cancel{O(\eta_n^2)} \quad \text{small}$$

Results in a familiar form

$$\eta_{n+1} = \lambda \eta_n \tag{3}$$

Intuitively, convergence and divergence depends on λ, or $f'(x^*)$, being smaller or greater than one. We can describe the stability of this point x^*. [5]

More importantly, cobweb graphs allows us to see the global behavior of linearization which helps support the local information of linearization. We can extrapolate if a systam is globally stable with cobweb analyzers. [5]

We introduce cobweb graphs as a way to visualize these stabilities. Plot the function $f(x_n)$ with the diagonal $x_{n+1} = x_n$. We plot through the iterative map $x_{n+1} = f(x_n)$ beginning at x_0. Alternating between moving vertically to the $f(x_n)$ function and horizontally to the diagonal line $x_{n+1} = x_n$. This gives indication of stability of this system (where to points converge and diverge given a starting value) [5].

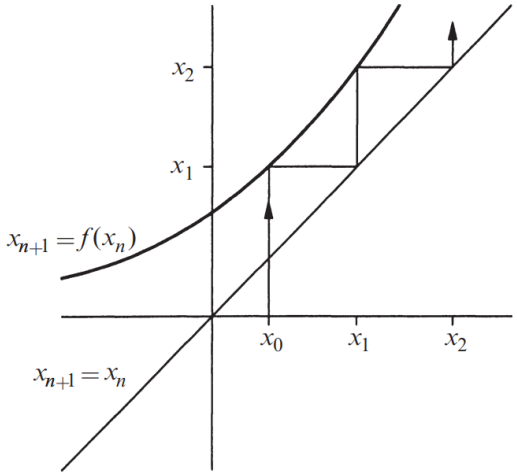

Figure 3: Cobweb Graphing more clearly illustrated. We iterate through $x_{n+1} = f(x_n)$ in a staircase ladder. [5]

For functional iteration, we know that we can find the nth element of a function $x_n = f(f(..f(f(x_0))...)) = f^n(x_0)$ [1]. There is an example of simple iteration with complex schemes with random number generation. The random number generators can create the successive almost random number by a certain and definite transformation on the current almost random number. So, a function is essentially going to be reevaluated successively to produce a sequence of the almost random numbers.So, if f is the function and x_0 is a starting number then we can find the next sets of numbers through the transformations.

1.1.3 Liapunov Exponents

Fundamentally, attractors are sensitive to the initial conditions. In other words, small variations will amplify and soon lead to drastically different results.

More formally: if you have points $\boldsymbol{x}_0$ and $\boldsymbol{x}_0 + \boldsymbol{\delta}_0$ s.t. $\boldsymbol{\delta}_0 \sim 10^{-15}$ etc.

$$\boldsymbol{x}_0 \to \boldsymbol{x}(t)$$
$$\boldsymbol{x}_0 + \boldsymbol{\delta}_0 \to \boldsymbol{x}(t) + \boldsymbol{\delta}(t)$$

The displacement vector vaguely grows exponentially and the points diverge away.

$$\|\boldsymbol{\delta}(t)\| \approx \|\boldsymbol{\delta}_0\| e^{\lambda t} \tag{4}$$

Call this λ the Liapunov exponent [5, p. 328]. It's important to mention some caveats. This relationship doesn't 'exactly' map the diverging trajectories – there is often pertubations and noise when they diverge exponentially. Additionally, this approximate relationship only works on the microscale – there is unavoidable error after a while [see 5, p. 328].

We can then use this above to formally find a more rigorous definition for λ:

$$\lambda \approx \frac{1}{n} \ln\left(\frac{\delta_n}{\delta_0}\right) = \frac{1}{n} \ln\left(\frac{f^n(x_0+\delta_0) - f^n(x_0)}{\delta_0}\right) = \frac{1}{n} \ln\left((f^n)'(x_0)\right) \tag{5}$$

$$\approx \frac{1}{n} \sum_{i=0}^{n-1} \ln\left(f'(x_i)\right) \tag{6}$$

$$= \lim_{n\to\infty} \frac{1}{n} \sum_{i=0}^{n-1} \ln\left(f'(x_i)\right) \quad \text{[see 5, p. 374]} \tag{7}$$

With a computer, we use this relationship to iterate for n times and approximate the liapunov exponent. In our lab, $f(x_i)$ is dependent on a chaotic parameter r so we can plot the λ vs r, iterating n times for every value of r that we plot (check Figure 10).

1.1.4 PN Junctions

The PN Junction allows current to flow in only one direction by through a diode with p-type and n-type semiconductors. These intersections exhibits properties of non-linearity which we'll use to study bifurcation of 2^n cycles.

$$C(V_d) = \begin{cases} C_0 e^{eV_d/kT} & V_d > 0 \\ \frac{C_0}{\sqrt{1-e^{eV_d/kT}}} & o.w. \end{cases}$$

We also know that the total current I does not depend on x because the current coming in the diode comes out the other end and the current is always continuous.

Substituting into linear elements of the circuit

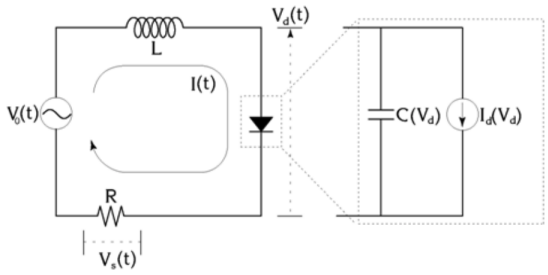

Similar to the logistic map, the wavefunction $V_0(t)$ will undergo bifurcations in this 2^n period doubling.

The **PN Junction** behavior can be made by putting donors into a P-type semiconductor and then subsequently this donor converts the P-type semiconductor into an N-type.

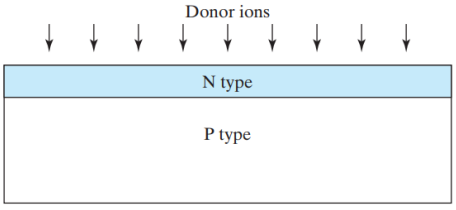

FIGURE 4–1 A PN junction can be fabricated by converting a layer of P-type semiconductor into N-type with donor implantation or diffusion.

This source is from Chapter 4 of Chenming Hu's textbook. [2]

Poisson's equation is an important aspect of the PN Junction because it relates the electrostatic potential to the net charge density within the depletion region.

$$\frac{d^2\phi(x)}{dx^2} = -\frac{\rho(x)}{\epsilon} = -\frac{q}{\epsilon}\left[N_D^+(x) - N_A^-(x) + p(x) - n(x)\right]$$

1.1.5 Bouncing Ball

The bouncing ball experiment is a digital circuit that simulates a ball bouncing on a vibrating surface in one dimension. In Newtonian mechanics, we can use the free fall equation for the Nth impact with the ground, where the ground is moving [8]:

$$x_{0T}\sin(\Phi_N) + v_N t_N - \frac{1}{2}gt_N^2 = x_{0T}\sin(\omega t_N + \Phi_N)$$

We have a phase offset Φ_N for every bounce on the ground. This phase updates every new bounce:

$$\Phi_{N+1} = \Phi_N + \omega t_N$$

We similarly use a weight on the velocity produced from freefall with the motion of the virtual ground:

$$v_{N+1} = K(gt_N - v_N) + (1+K)\omega x_{0T}\Phi_{N+1}$$

Mathematically, we can discover a world of chaotic regimes under adjustments to K and $\alpha = \omega^2 x_{0T}/g$. These adjustments reveal similar chaotic systems studied in the logistic map 2, as shown in Figure 5.

We can translate these analytic equations into circuit elements. For example, we use a cascade of integrator op-amp circuits [8].

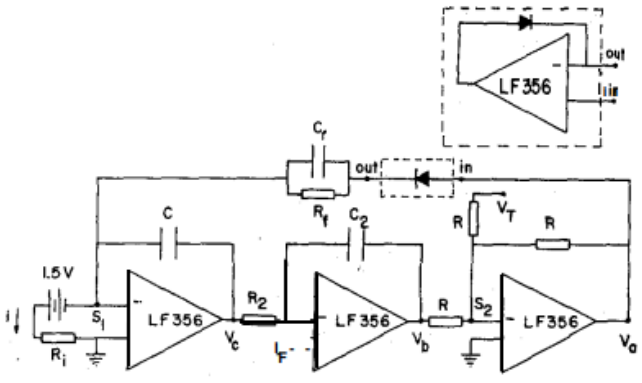

Figure 4: Modeling the components of the equations above with component elements [8]

Upon measurement, we can see that the process undergoes a familiar process of bifurcation and chaos regimes found in the logistic map 2.

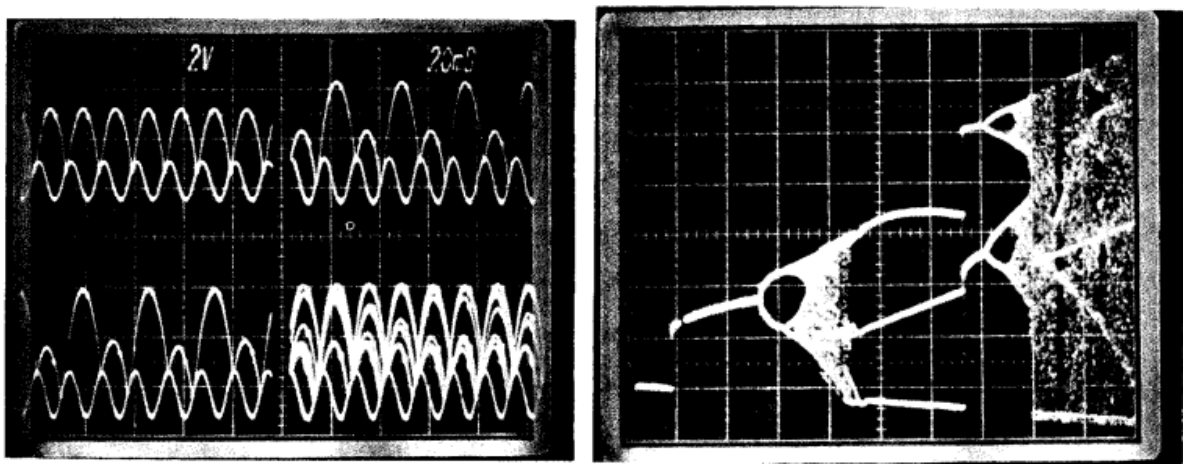

Figure 5: Oscilloscope readings of the bouncing ball experiment taken from Zimmerman [8]

2. Procedure and Analysis

2.1. Power Spectral Density Plots in LabView

Using LabView 2025, we created a new VI program to read a voltage signal from the DS345 Wave Generator, which is a wave function generator that uses digital synthesis to create sine, square, triangle, and ramp waveforms, etc. To do this we attached attached the exiting signal directly to computer interface box, which is an enclosure around a DAQ that feeds into the PC.

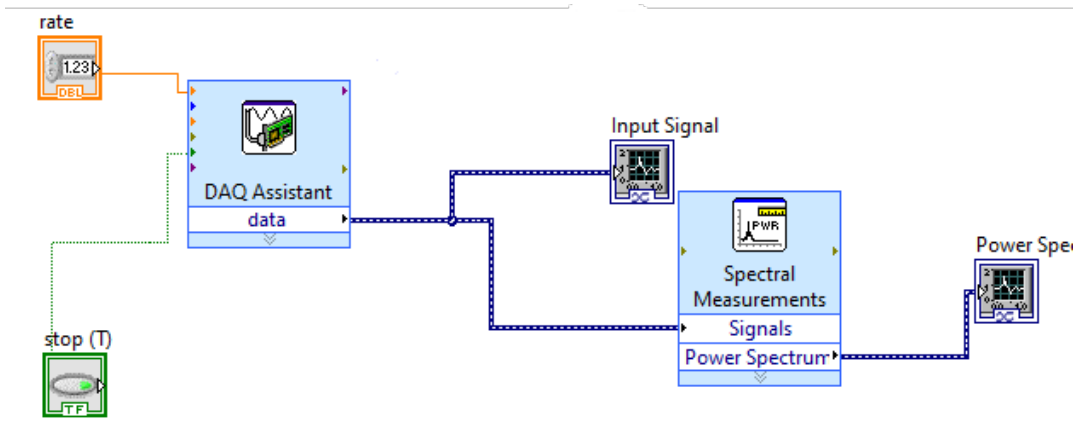

Figure 6: Block Diagram of the LabView sampling of a sinusoidal wave produced by DS345 Wave Generator

We write a simple LabView script to collect and plot in Figure 6. The DAQ assistant provides data that we plot directly as the 'Input Signal' (not depicted below) and process using LabView's Power Spectrum module for plotting.

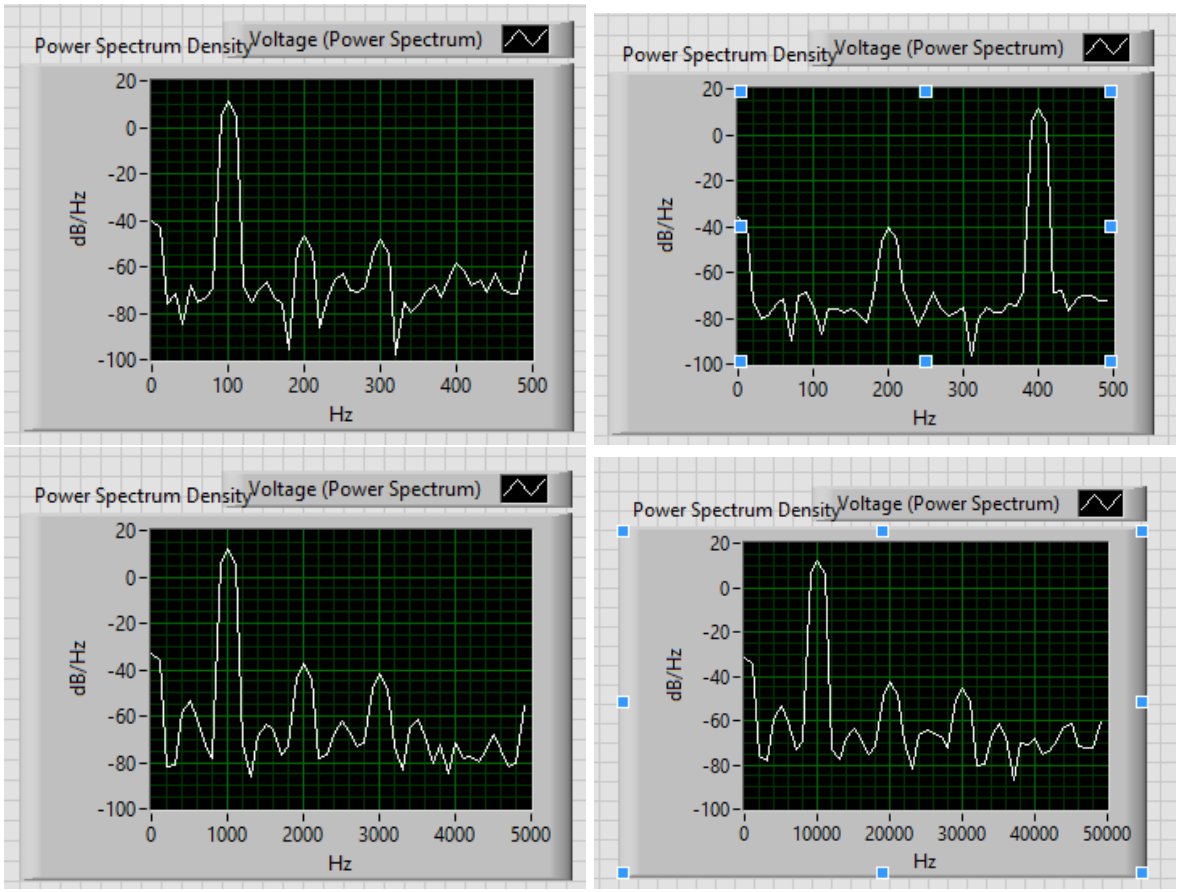

Figure 7: Plotting Power Spectrum Density from the sinusoidal wave produced by the DS345 Wave Generator at 100Hz, 400Hz, 1kHz, and 10kHz.

In Figure 7, we can see spikes centered around the frequency we've set by the function generator, which aligns as this ultimately shows the frequencies with higher and lower power density. [7, pg.] However we also see nontrivial noise in neighboring frequencies from the DS345 and the pipeline into our data collection.

2.2. Cob Web Analyzer

In LabView 2025, we write a new VI program that generalizes the Cob Web algorithm. Our specific cobweb algorithm demonstrates the effect of repeatedly applying a quadratic map to a given initial value of x. In the rectangular box in the lower part of Figure 8, we created N equally spaced values of x_n between 0 and 1 and fed this into $x_{n+1} = rx_n(1-x_n)$. Using these values we can plot both $x_{n+1} = x_n$ and $x_{n+1} = f(x_n)$.

In the upper part of Figure 8, we are generating the successive sequence

$$x_0, f(x_0), f(f(x_0)), ..., f^n(x_0)$$

by iterating through the quadratic map. We can use these values, interweave it with itself, replacing the first index with zero and removing the last two elements. This specific interweaving leaves us with all the iterative points of our cobweb graph 9:

$$\{x_0, 0\}, \{x_0, f(x_0)\}, \{f(x_0), f(x_0)\}, \{f(x_0), f(f(x_0))\} \tag{8}$$

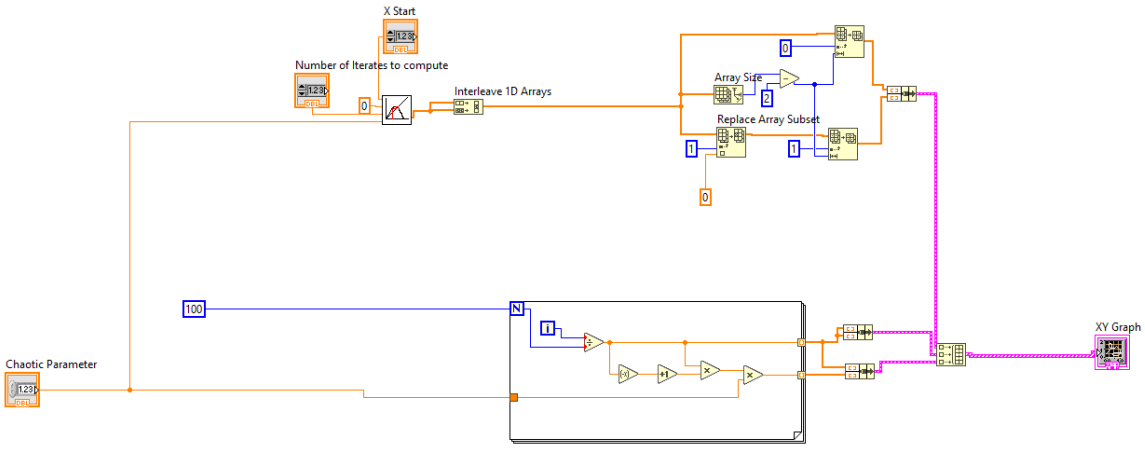

Figure 8: Custom CobWeb Analyzer VI running our logistic map eq. 1

We plot the points from above 8 under a reasonable parameter such as $r = 2.86$ and an initial $x_0 = 0.16$. We see a spiraling convergence to a point.

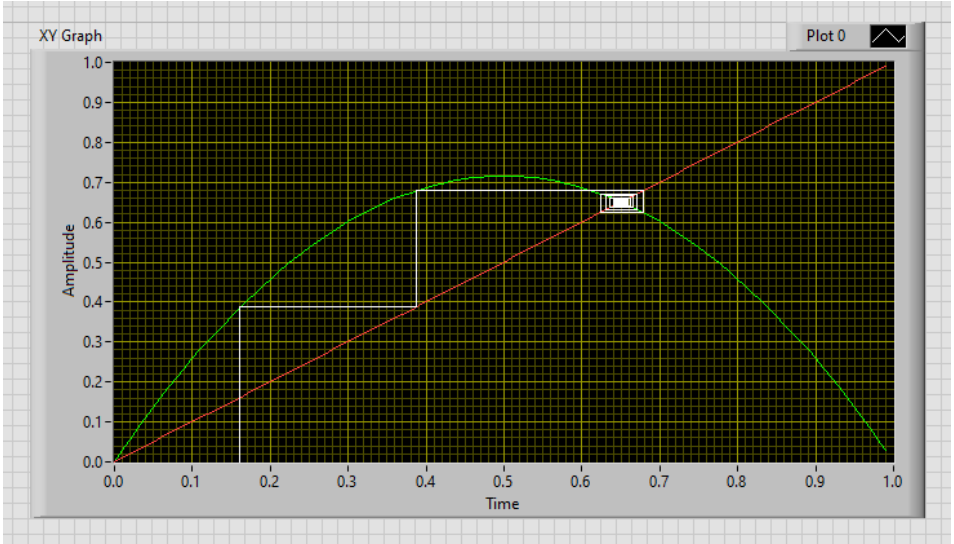

Figure 9: The cobweb graph of the logistic map eq. 1 iterating 1000 times with a chaotic parameter of 2.86

This spiral implies the point converges with damped oscillation; it mimics a spring-mass system by oscillating past and before the 'equilibrium' value.

Relating back to the logistic map, by calculating $f^n(0.16)$ via successive iteration of our quadratic map, we can see this damped oscillatory convergence onto our stable point in the first graph of Figure 1. This stability occurs because of our chaotic parameter is set slightly below 3, which excludes any of the 2^n cycle oscillations as seen in Table 1 – 'population' converges with this r.

With a chaotic parameter increase slightly above 3, we can see the cobweb ultimately falling into a rectangular loop, alternating between two values of x. Matching the second graph of Figure 1. This system has two stable points and the LabView plot shows that.

With a chaotic parameter increased slightly higher to $r = 3.43$ i.e., we fall into the expected period-4 cycle. There are two loops that alternate the value between 4 values as seen in the third graph of Figure 1.

Finally, with $r = 3.9$ we find no defined behavior in the cobweb graph. The lines are plotted all over.

2.3. Liapunov Exponents

In this section, we sought out to calculate the Liapunov exponents of the logistic map as a function of its chaotic parameter with an underlying python script and LabView's graphing utility. The script follows eq. 6; it iterates n times for a given value of r to numerically determine λ. The components are not particularly difficult – with $f'(x_n) = r(1 - 2x_n)$. We can repeat this for various a set number of r and graph.

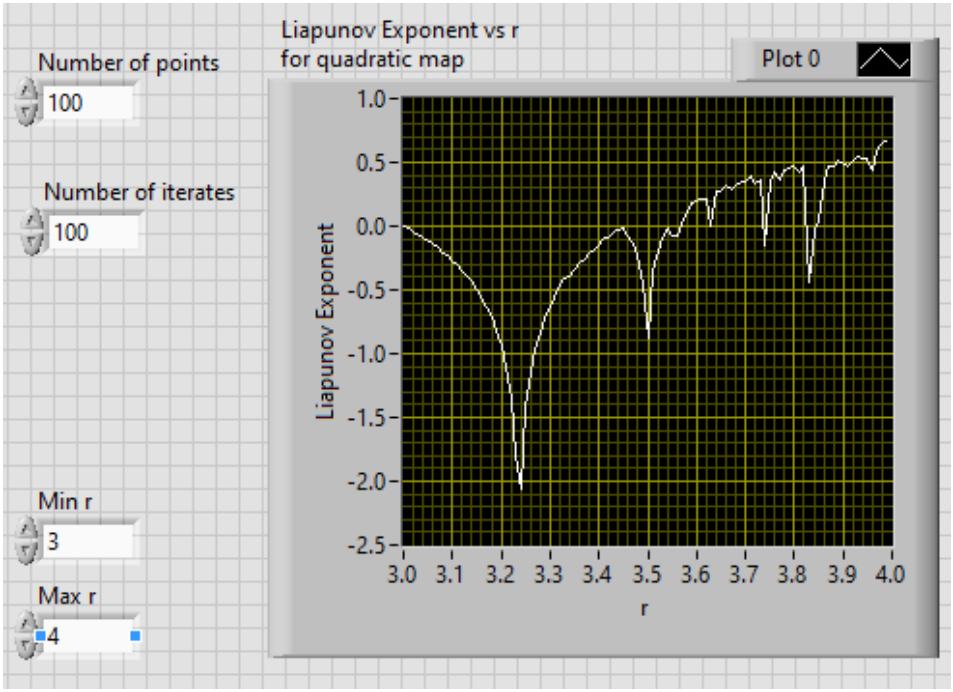

Figure 10: Sampling the Liapunov exponent for our logistic (quadratic) map which matches the textbook solution in Strogatz [5]

Take a look at the known points of the period cycles of the logistic map in Table 1. Notice that they correspond to the parts on the graph where $\lambda(r) = 0$. We can see these separating the initial different 2^n cycles.

Additionally, recall that $\lambda < 0$ suggests a convergence behavior of nearby points and $\lambda > 0$ means a divergence behavior from as shown in our introduction 4. These sections where $\lambda < 0$ correspond to global stability such as the period 2 cycle, with a peak stability at around $r = 3.24$. These peaks just determine chaotic parameters where the 'damping factor' is highest on the oscillations into convergence (in first graph of Figure 1). Similarly, we find peak period-4 cycles at around $r = 3.5$.

Recall from the Table 1 that chaos begins at around $r = 3.57$. This corresponds to the part of the bifurcation graph 2 that explodes into a chaotic mess. This also corresponds to the point on the Liapunov exponent graph where $\lambda > 0$. Intuitively, this makes sense since eq. 4 shows that nearby points are diverging away from this instability point.

Note that past the point of $r = 3.57$ there are yet again momentary dips under $\lambda < 0$. These correspond to moments of stable oscillations found in the logistic map graph 2. For example, we find a particularly whimsical moment of 3-cycle at $r = 3.83$ which corresponds to the dipped peak in the Liapunov graph at $r = 3.83$.

2.4. Nonlinear Dynamics Simulations

2.4.1 Sinusoidal

Before actually running nonlinear systems with circuit elements, we can simulate nonlinear system in LabView. In the NLDSIM.VI program, we simply simulate a few functions and three graphs are produced, a time-series graph, a return map, and a power spectrum. As a starting off point, we run the function $x(t) = \cos(\omega t)$ which mirrors the setup we had in the first section 2.1.

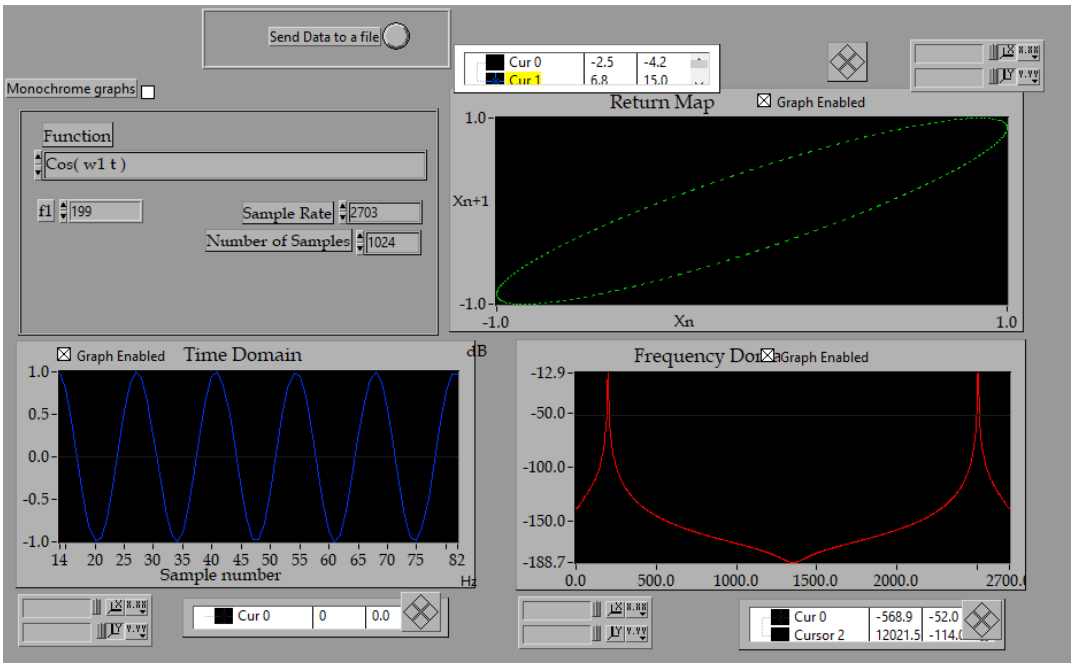

Figure 11: NLDSIM program plotting a simple cosine wave in the time domain, frequency domain, and return map.

The time-domain graph in Figure 11 graphs the actual function we are plotting. In this case that is $x(t) = \cos(\omega t)$. The frequency power spectrum shows us the power density of certain frequencies found as a function of amplitudes of certain frequencies [7]. This plot makes sense as its a delta function around $\pm\omega$. The return map plots x_{n+1} vs x_n which describes the $x_{n+1} = f(x_n)$ from before 2. This is thus a Poincare map as it samples a section of the continuous function $x(t)$.

Notice how this is an ellipsoid which means this function has a cyclical period – the function $x(t)$ eventually repeats itself.

Before moving on, we'd like to note that a very large sample rate can skew the results. By increasing the sample rate for this specific program, we are taking a smaller interval but more closely spaced compared to its frequency.

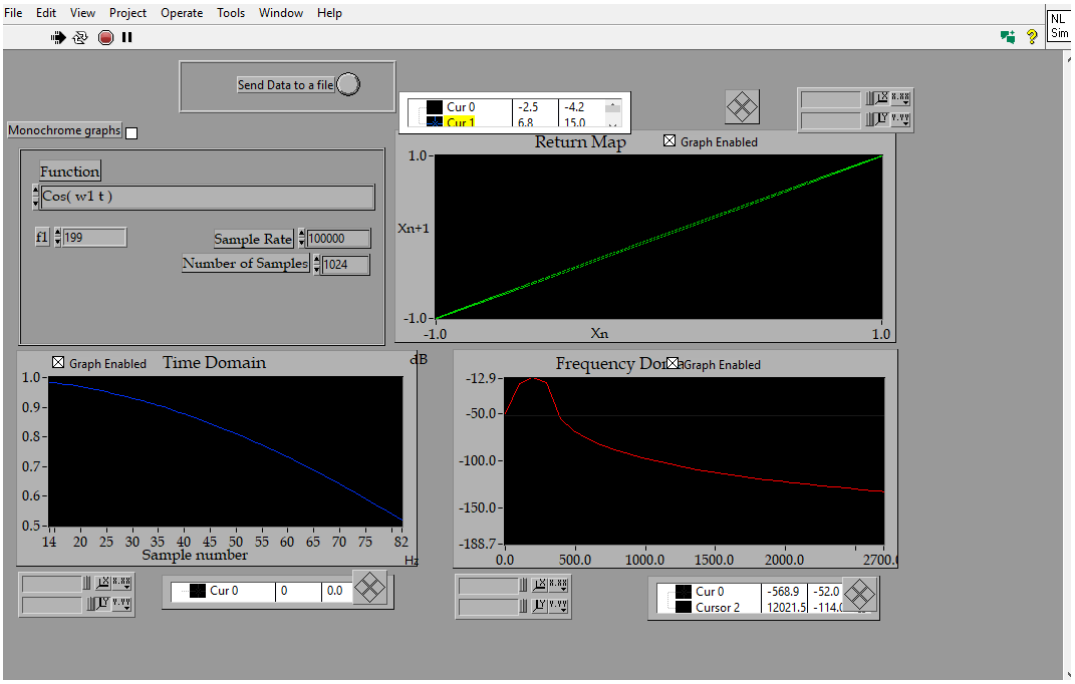

Figure 12: NLSIM graphs with a large sample rate skewing results

This high sample rate effectively removed the previous cycle in the input signal. Additionally, points are closely knit so x_{n+1} and x_n are closely together. Hence, the Poincare map drifts towards $x_{n+1} = x_n$ diagonal.

The frequency shows a very low fundamental frequency – a large hump near zero – which matches the time domain signal.

2.4.2 Sum of Sinusoidals

Next, we ran the function of the sum of cosines seen below. For Poincare sections we know that if the ratio of frequencies 1 and 2 are rational, the return map shows a recursive, finite set of points. This is a scenario in which we would be seeing a cycloid in the return map, because cycloids are recursive pattern of points. When the frequency ratio is irrational, then you will begin to see a torus because the trajectory of points created on the return map are not in a repeating pattern. When A is a nonzero term in the equation it adds a combined frequency term, and the system is still a two frequency dependent system.

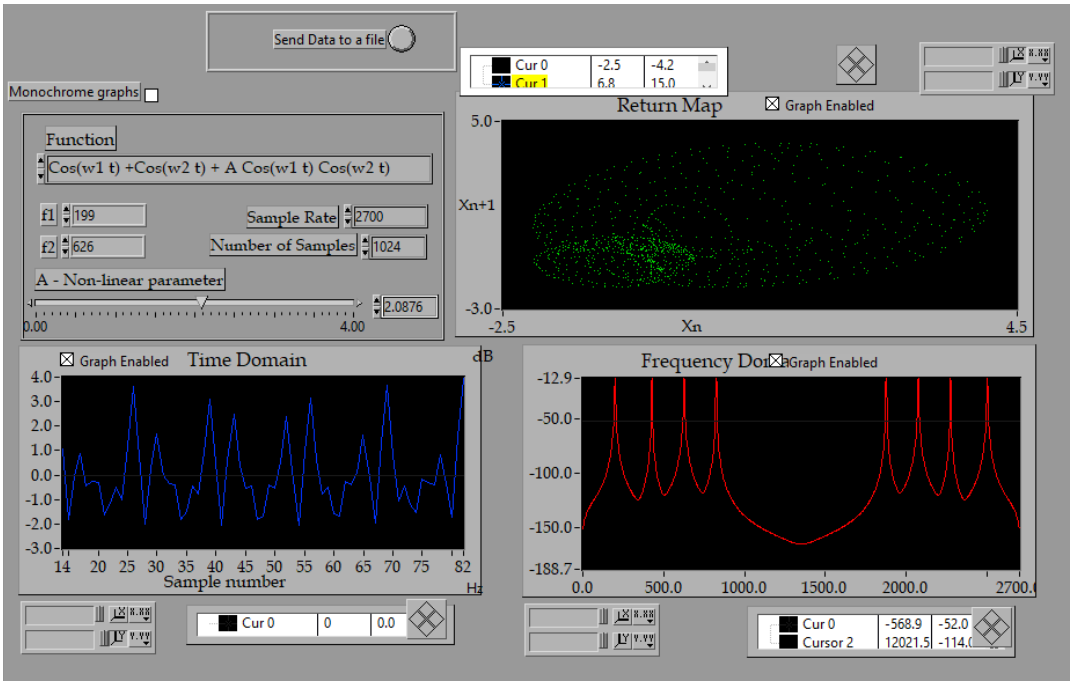

Figure 13: NLSIM graph as a sum of cosines: torus

This is not a chaotic system, instead it is periodic. We can observe that the system does not diverge dramatically with small changes to initial condition. The system can really only produce two outcomes, a torus with an irrational frequency ratio, or a repetitive continuous cycloid.

In the time domain, for the torus shape, the shape does not exactly repeat, but it is still semi-periodic. For the cycloid shape, there is a clear periodicity in the time domain. In the frequency domain the cycloid shape displays pulses at an integer multiple of frequency 1/T. In the frequency domain for the torus shape there are peaks at each frequency then peaks at sums of the frequencies.

2.4.3 Further Discussion

The axes of the return map are represented by the Nth state (X-axis) Vs. The N+1th state (Y-axis). So it is plotting the successive points of the system. They are the values of the system at a given time step. The shape of the paths in the phase space for this system is represented by an ellipsoid, which is what we see in the return map.

When we make the sample rate very large, the return map goes to a line, which means that the change from the return value from one state to another is very small. When we minimize the sample rate, the chaotic behavior increases and the points become more pseudo-random. When we increase the sample rate, the return map narrows around the diagonal since points are almost the same in such a small interval and we get closer to the relation $x_{n+1} = x_n$. When the sampling rate is a multiple of the frequency of the cosine we know from the Nyquist criterion that the Nyquist frequency determines the stability of dynamic systems. If you sample at a high integer multiple of the frequency you can ultimately eliminate aliasing,

As explained in the theory, in the time domain for the torus the shape does not repeat but it is semi periodic. For the cycloid, there is periodicity in time domain and in frequency domain the cycloid shape displays pulses at an integer multiple of frequency. In the frequency domain for the torus there are peaks at each frequency then peaks at sums of each frequency.

2.4.4 Logistic Map

Next we worked on the quadratic map function and examined the map's behaviors under various r parameters. When r was set to 2.8, the return map displayed a singluar point which is hard to grasp in Figure 14. As discussed before 1, when $r < 3$, we have complete stability in the system. As shown, the values converge towards a singular x_n. This matches the singular point in x_n vs x_n space. In addition, we see $x(t)$ converging onto a straight line in time domain just as the textbook case did in the first graph of 1.

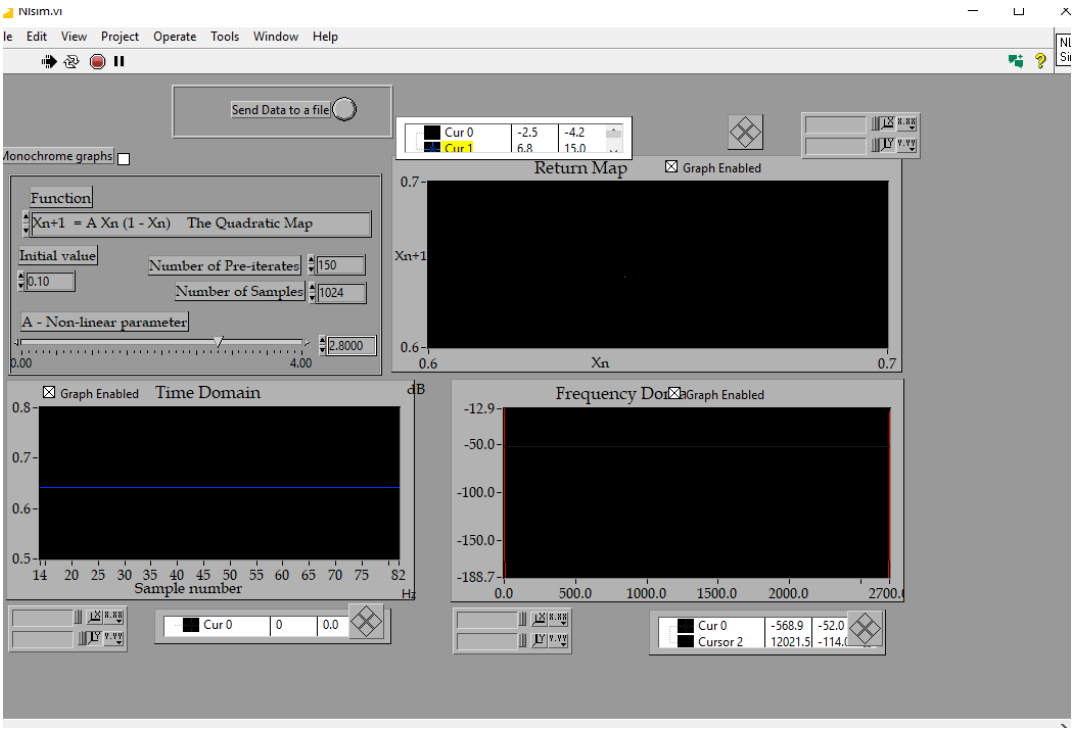

Figure 14: Quadratic Map r = 2.8

As we increase r, we'll see the first splitting into the 2-cycle. Once again, this time domain signal coresponds to the textbook example in ref. 1. The input signal clearly shows an oscillation between two values. We can see the rough mapping between them on the return map (although ideally it would be appear like two points on the return map. This just shows that the liapunov exponent is not at its peak and there exists a low damping factor). Additionally, we can see a solid delta function at the frequency of this 2-cycle oscillation.

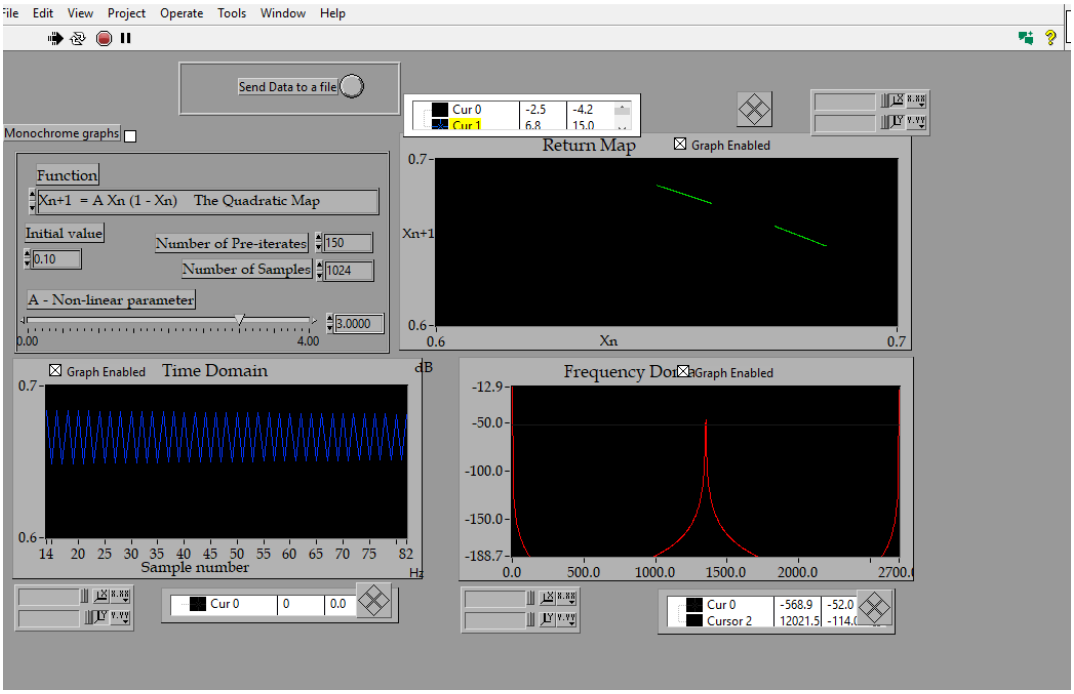

Figure 15: Quadratic Map r = 3

Increasing $r = 3.5$ gives us 4-cycle. The input signal in the time domain displays an alternating between 4 values, which matches the textbook reference 1. Our return map shows exactly 4 points (you'll have to zoom in to see). These are the stable points that the system converges into. The frequency domain displays the superposition of these frequencies to produce the input signal.

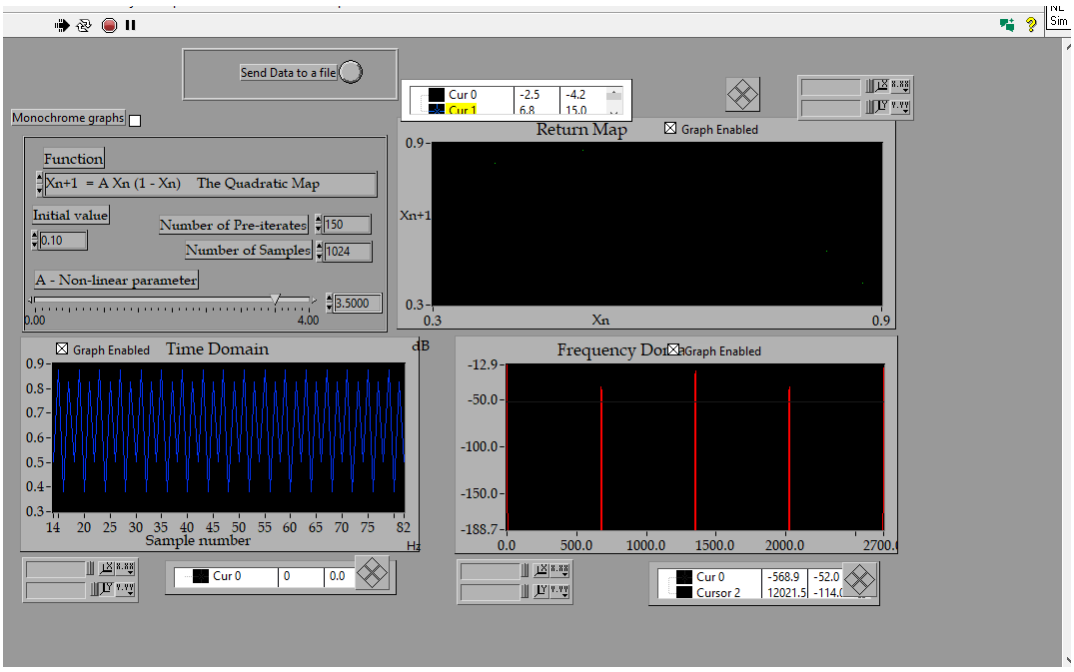

Figure 16: Quadratic Map r = 3.5

Finally, increasing to $r = 3.56$ reveals 8-cycle. Similar to the example above we see 8 points on the return map that the values are oscillating between (may be hard to view).

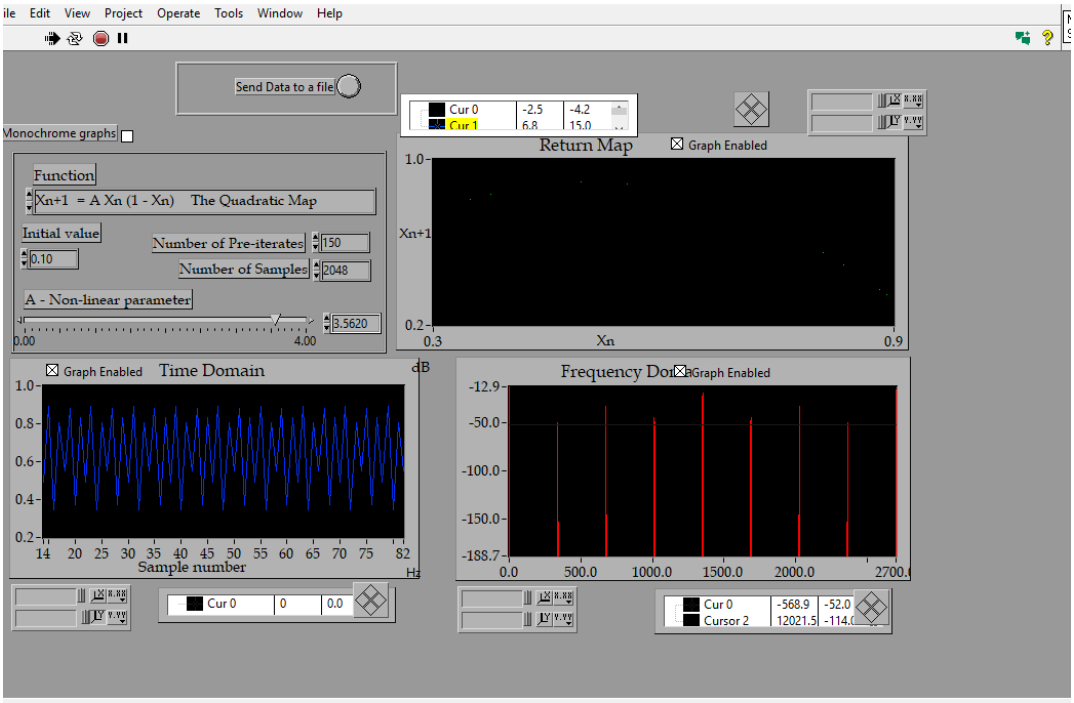

Figure 17: Quadratic Map r = 3.56

2.4.5 Henon Map

Finally, we worked on the Henon Map. In the return map of the Henon Map the anamoly seen is a culmination of a previous value and a squared value attractor, where the Henon Map does loop back into a periodic signal. The Henon Map is a fractal where it is smooth in one direction and the other direction is a cantor set. A cantor set is a frcactal that is creating by removing the middle third segment and then repeats that iteration on successively smaller segments,

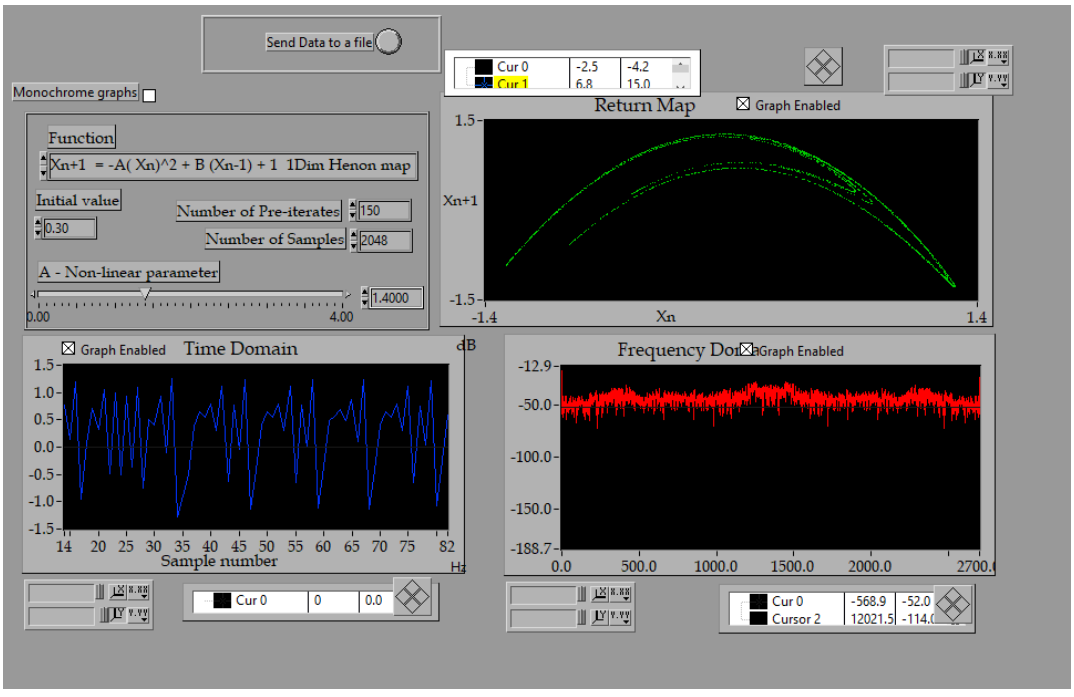

Figure 18: Henon Map

The strange thing seen in the Henon Map is the strange attractor which represents a chaotic fractal bending of the graph that resembles a warped boomerang. Although the graph appears to be a simple curve, upon further inspection one can see a set of parallel lines making up this shape. These parallel lines in actuality are a single infinite line that is locally chaotic but globally stable. The Strange attractor seen in the Henon Map is made by a repeating process of a non-linear folding that is occuring, which ultimately causes an exponetional divergence of nearby points while still being able to remain in a bounded region. Taking the cross-section of the Henon Map reveals a Cantor Set structure which means it is a series of points making up the curve instead of a smooth line. When we take the dimension of the graph, we get a dimension of about 1.26 as reflected in our dimension section.

The Henon Map which is defined by $x_{n+1} = 1 - ax_n^2 + y_n, \quad y_{n+1} = bx_n$ shows a transition between from stability to chaos through period-doubling which cascades as the a parameter is varied, and the b parameter is generally set at about 0.3. The Henon Map behaves as a 2D prototype of folding behavior which starts from an initial fixed point, then 2 cycle then 4 cycle and eventually chaotic behavior.

2.5. PN Junction

We begin to examine the PN-Junction system in a nonlinear circuit 1.1.4. Luckily the NLD circuit setup is designed. In Figure 19, we demonstrate our experimental wiring. We used the model DS345 Stanford Drive Oscillator to feed into the external reference node of the computer. After setting up all the connections, the NLDGEN.VI program collects the data via DAQ and we were able to see a time-series, a Fourier Power Spectrum, and a return map. We used a 30kHz sampling rate and set the DS345 Wave Gen to 3.5 kHz 10-volt sinusoidal wave.

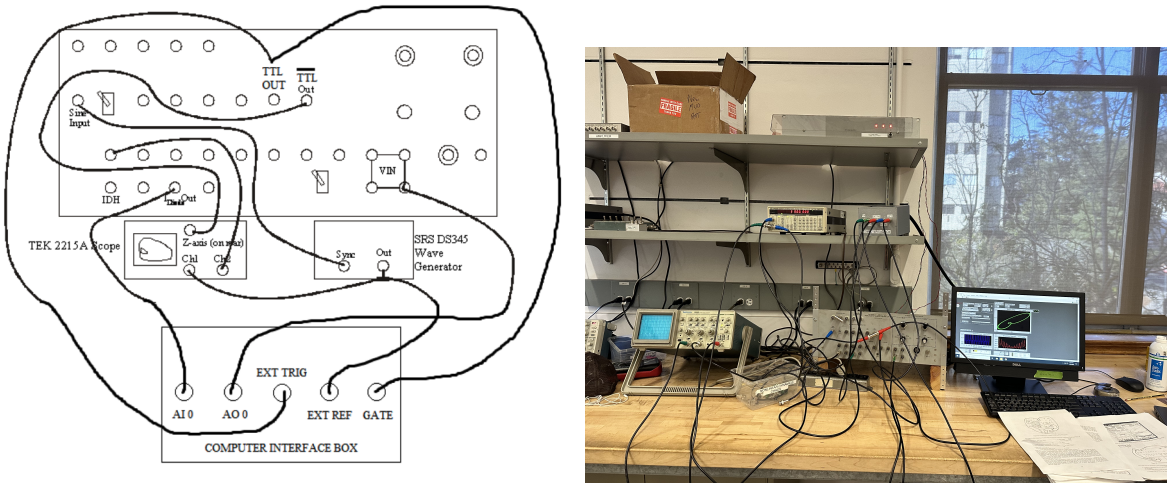

Figure 19: PN Junction Setup

This sets us up to view and analyze plots of a PN-junction circuit driven by a sinusoidal wave. We can see an example of this in the Figure 20 below.

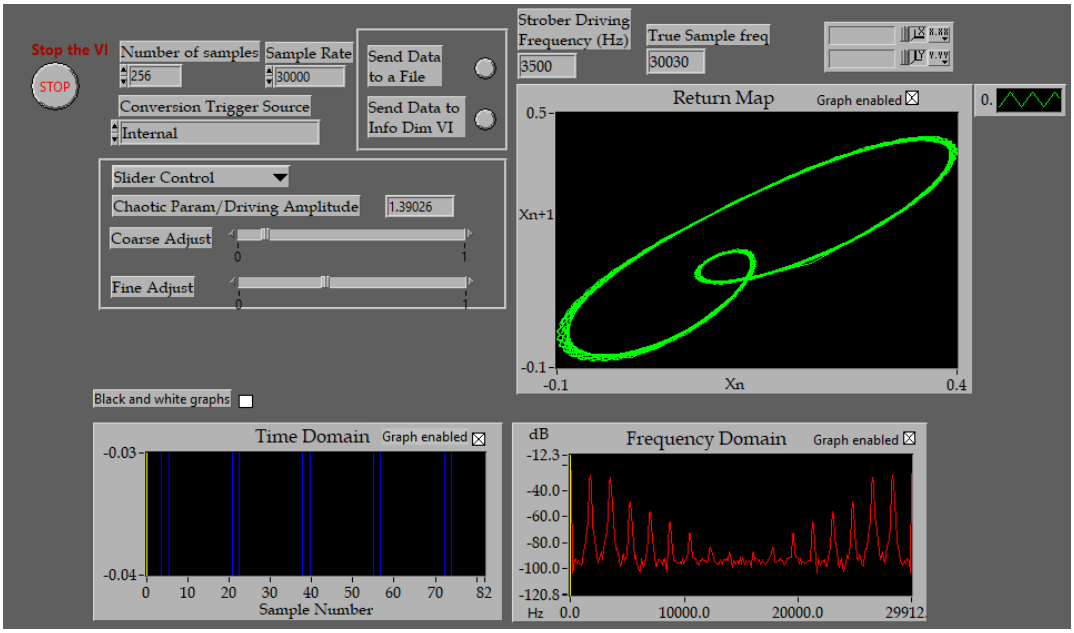

Figure 20: Bifurcations

Upon examination, we can see that the return loops back which implies the signal in the time domain has a cycle. More specifically, this particular Poincare map is in a 2-cycle.

Additionally, we can see strong peaks in the frequency domain in both directions. We can assume that the Liapunov exponent is $\lambda < 0$ and strong such that these frequencies are obvious and uncluttered by noise.

We further our experiment by adjusting the chaotic parameter below:

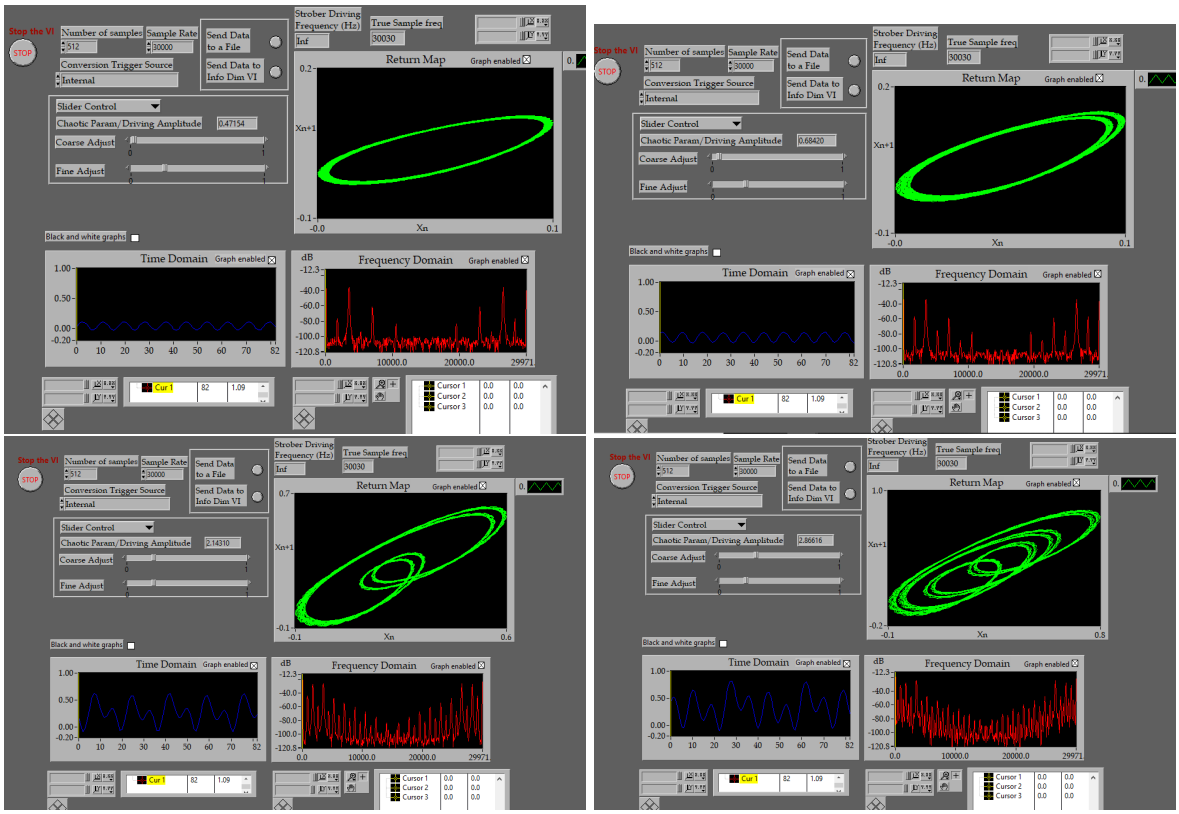

Figure 21: PN Junction Period Doubling

In the first graph's time domain in the Figure 21 above, we can see the simple sinusoidal wave we are passing into the system via the DS345 Wave Generator. This matches the results from Figure 11 before except current setup is based on experimental data rather than simulated data.

As presented, the graphs undergo a series of bifurcations characteristic to the period-doubling we've seen in the quadratic map. Specifically, the sinusoidal wave function we passed into the circuit system begins to separate into superposition of waves. Additionally, the return map loops we've seen also bifurcate as seen in other examples such as Duffing's equations or Lorenz's equations [1]. In fact, period doubling systems have a 'Universal Behavior' characterized by Feigenbaum that all share a ratio [1].

I'd like to note that all this was created via the diode's nonlinear PN junction in response to a sinusoidal input which result in a unique bifurcations we don't have an analytic solution to on hand. These data are completely experimental.

Estimated Chaotic Param	Period
0.67	2
2.14	4
2.80	8

Figure 22: Period doubling at certain chaotic parameters measured experimentally.

These period doublings continue. The universal feigenbaum ratio also holds in this period doubling experiment even though we've studied the logisitc map up until this point [6].

2.5.1 Chaos and Entropy Discussion

As anticipated, increasing the chaotic parameter in Figure 21 above would result in a mess of points on the return map with no particular pattern. We characterize these sections as chaotic as the sheer number of possible unique x_n which lower the Shannon Informational Entropy $-\sum p \log p$ [4]. In turn, it becomes impossible to transmit information since there are so many unique possible values or 'bin' as illustrated by May [3]. In other words, in these chaotic regions, we develop noise.

2.6. Bouncing Ball Experiment

We use the following setup for the bouncing ball experiment detailed in Zimmerman [8] which can be summarized in the theory section above. We have an electronic setup already which we wire according to Figure 23 below.

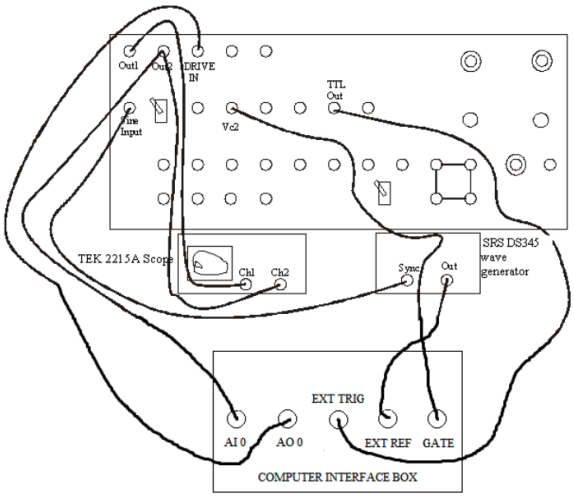

Figure 23: Bouncing Ball Block Diagram

We setup with the following parameters: 0.05 EP Resolution, 0.125 EP Max, Embedding Dimension 2, Number of Points 1024, Elapsed Time tau 1, Near Neighbors 1.

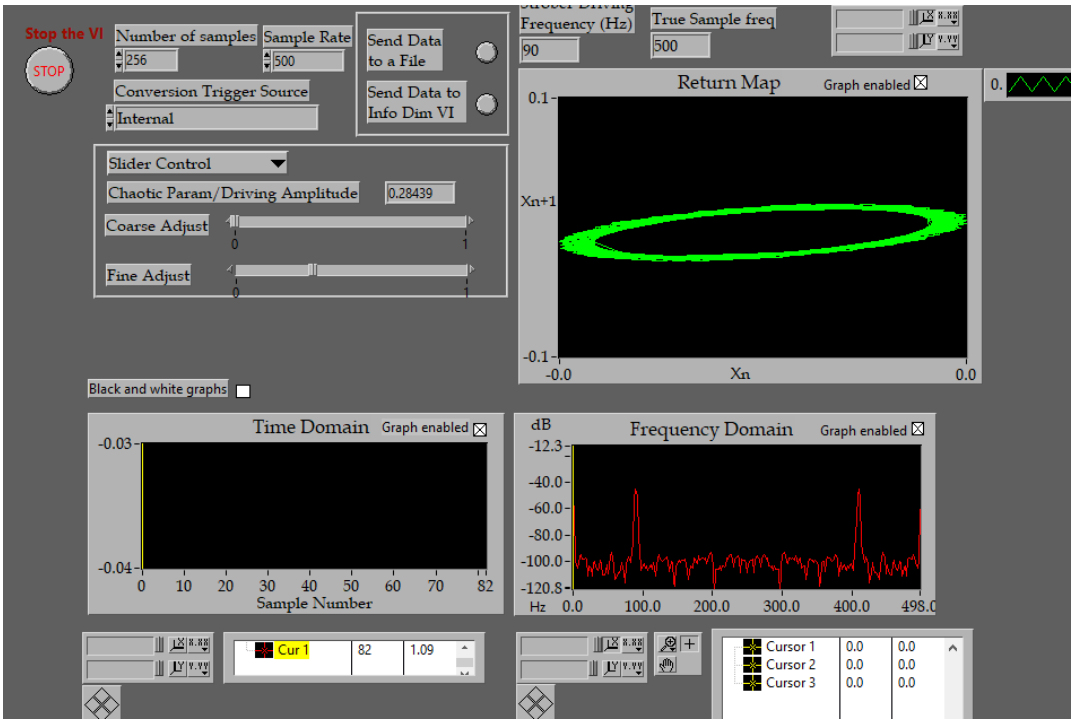

Figure 24: Bouncing Ball with r = 0.28

Starting off, we set our chaotic parameter low. Similar to the PN junction seen in the previous section, we can see a relatively strong sinusoidal wave across all three plots. This base case example roughly matches what we've seen in NLDSIM 11 and PN Junction Base Case 21.

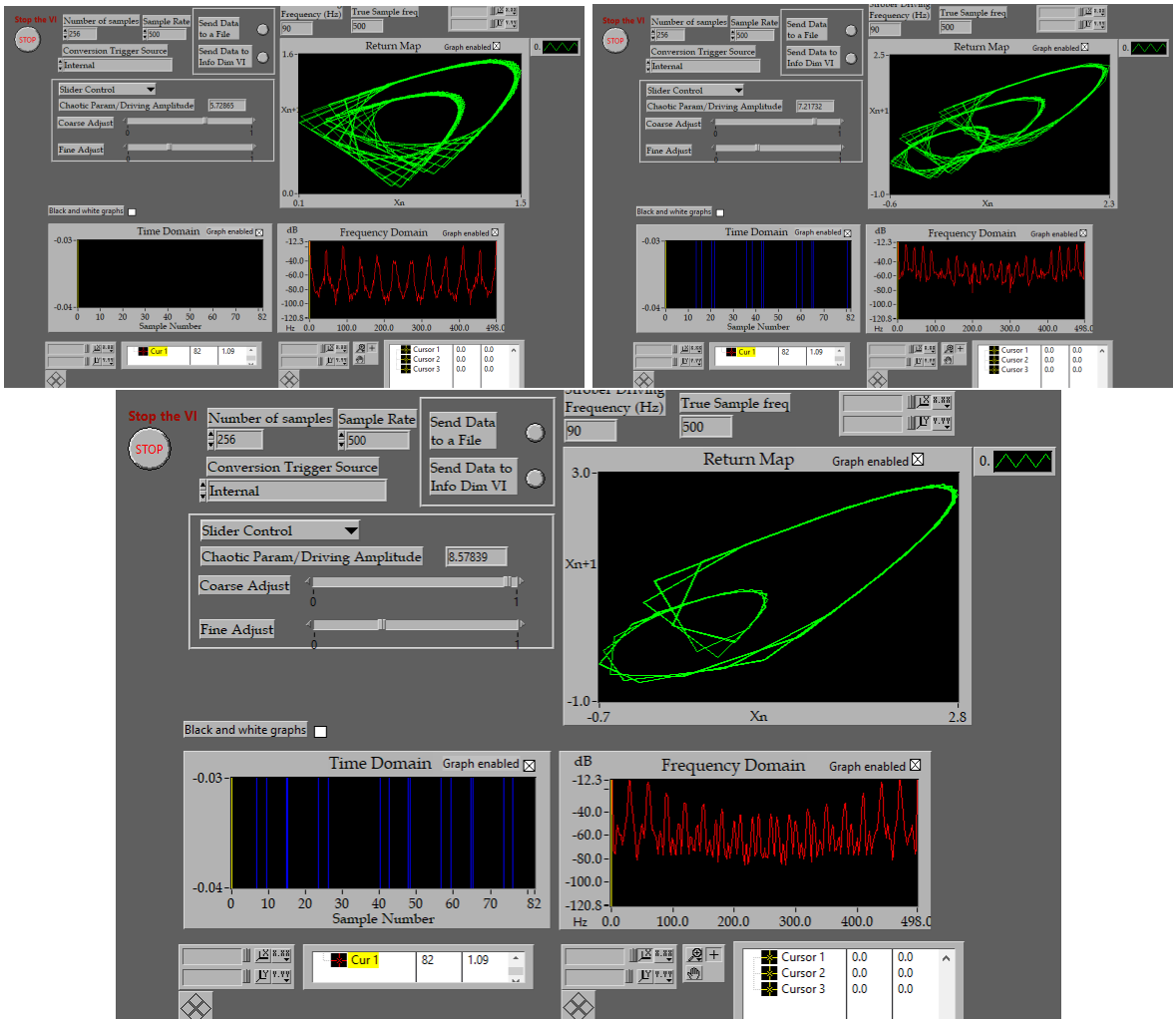

Figure 25: Bouncing Ball at r = 5.7, 7.2, 8.5 respectively

Similar to PN Junction period doublings 21, we also see very similar bifurcation process. We see loop split in the first graph. However, strangely we get a three cycle and later a 2-cycle loop. These results matches exactly the textbook bifurcation diagram in Zimmerman shown in the introduction 5. Moving along the horizontal, we can see the 2-cycle, 3-cycle and later 2-cycle that this specific bouncing ball experiment produces.

Note, the time-domain appears hard to read. Quite possibly, the graph was scaled incorrectly but we should see a wave of some sorts produced by the 'simulated' bouncing of a ball on the vibrating virtual ground. For this case, please ignore the time-domain.

We can see the frequency domain changes similar to how the PN Junction. We have what appears to spiky peaks, almost noise. Then the higher frequency peaks begin to dominate as we bifurcate. This makes sense as the oscillations within the input signal should contain more smaller period cycles within. For example, we see small bifurcations 'forks' in the logistic map graph 2.

Recall that these are all just electronic circuits. While this common experiment has been studied extensively, we've let the experiment run, collect the data in LabView and study the results.

3. Conclusion

The experiment of NLD successfully investigated the behaviors of chaotic systems to observe and examine the transitions from periodicity to chaotic behavior as we experimented with driving amplitudes and voltages. Our results were constant with the idea that an increase in voltage can lead to a period doubling cascade. The bifurcation diagram clearly showed bifurcation points at 3.56 which showed a rapid switch to chaotic non repetitive behavior.

References

[1] Mitchell J Feigenbaum. "Universal behavior in nonlinear systems". In: *Physica D: Nonlinear Phenomena* 7.1-3 (1983), pp. 16–39.

[2] Chenming Hu. "Modern semiconductor devices for integrated circuits". In: *(No Title)* (2010).

[3] Robert M May. "Simple mathematical models with very complicated dynamics". In: *Nature* 261.5560 (1976), pp. 459–467.

[4] Claude Elwood Shannon. "A mathematical theory of communication". In: *The Bell system technical journal* 27.3 (1948), pp. 379–423.

[5] Steven H Strogatz. *Nonlinear dynamics and chaos: with applications to physics, biology, chemistry, and engineering*. Chapman and Hall/CRC, 2024.

[6] James Testa, José Pérez, and Carson Jeffries. "Evidence for universal chaotic behavior of a driven nonlinear oscillator". In: *Physical Review Letters* 48.11 (1982), p. 714.

[7] Saul A Teukolsky et al. "Numerical recipes in C". In: *SMR* 693.1 (1992), pp. 59–70.

[8] Robert L Zimmerman, Sergio Celaschi, and Luis G Neto. "The electronic bouncing ball". In: *American journal of physics* 60.4 (1992), pp. 370–375.